JOURNAL OF SOLID STATE CHEMISTRY 15, 9–17 (1975)

The Effect of Crystal Size on Chemical Hysteresis in Praseodymium and Terbium Oxides

A. T. LOWE, K. H. LAU, AND L. EYRING*

Department of Chemistry, Arizona State University, Tempe, Arizona 85281

Received August 7, 1974

The effect of the variation of crystal size on chemical hysteresis in phase reactions has been investigated by means of thermogravimetric analysis. Series of isobars were followed at several different pressures and crystal sizes for the PrO_x–O_2 and TbO_x–O_2 systems. At higher temperatures the extent of hysteresis decreased with increase in crystal size for both oxides. It was found that equilibrium was not attained in reactions occurring at lower temperatures. These experiments are contrasted with previous investigations using powdered samples. Some plausible explanations for the trends observed are discussed.

Introduction

The study of the effect of particle size on the main features of phase reactions in rare earth oxide systems has recently been made possible by the availability of single crystals of praseodymium and terbium oxides grown by a hydrothermal technique (*1*). The crystallite sizes available for these studies range in diameter from 0.01 to 0.16 mm. This affords a diffusion path as large as three orders of magnitude greater than in the crystallites present in the powdered samples used previously.

A series of hysteresis scanning loops in the system TbO_x–O_2 (*2*) carried out in the composition interval between $TbO_{1.5}$ (φ phase) and $TbO_{1.714}$ (ι phase) indicated an intrinsic hysteresis unaffected by the rates of heating and cooling. It was proposed that the hysteresis was caused by a free energy difference arising from intergrowth domain interfaces. For the PrO_x–O_2 system there are similar indications that the loop between $PrO_{1.5}$ (φ and/or σ) and $PrO_{1.714}$ (ι) is also intrinsic. A determination of the effect of crystal size on chemical hysteresis in these intrinsic regions of the phase diagram was needed to further clarify the mechanism of this imperfectly understood phenomenon. Apparent also in the studies was a marked diminution of the rates of phase reactions at lower temperatures.

Each oxide system consists of a number of phases belonging to the homologous series R_nO_{2n-2} (Table I). In addition, the PrO_x–O_2 system exhibits wide-range nonstoichiometry at higher temperatures and oxygen pressures. The ordered intermediate phases and the nonstoichiometric phases are formed at easily accessible temperatures and pressures, making possible the investigation of a wide range of reactions. A series of isobars for powder samples in the two systems (*3*) are shown in Figs. 1 and 2.

Experimental

The oxide crystals used for all of the thermogravimetric experiments were hydrothermally grown from thermally decomposed nitric acid solutions by techniques described previously (*1*, *4*). The PrO_2 crystals were screened to provide samples with a small range of crystal sizes whereas the TbO_x crystals were mixed sizes as indicated in Table II. Examination of the crystals with secondary electrons in an electron microprobe

* To whom inquiries should be sent.

TABLE I

HOMOLOGOUS SERIES R_nO_{2n-2} IN THE PRASEODYMIUM AND TERBIUM OXIDE SYSTEMS

n	Phase designation	O/R ratio	Fraction of oxygen atom missing	Known members of the Pr–O	Tb–O
4	Sesquioxide	1.5	$\frac{1}{4}$	Pr_2O_3	Tb_2O_3
6	κ	1.667	$\frac{1}{6}$	Pr_6O_{10}	
7	ι	1.714	$\frac{1}{7}$	Pr_7O_{12}	Tb_7O_{12}
9	ζ	1.778	$\frac{1}{9}$	Pr_9O_{16}	
10	ε	1.800	$\frac{1}{10}$	$Pr_{10}O_{18}$	
11	δ	1.818	$\frac{1}{11}$	$Pr_{11}O_{20}$	$Tb_{11}O_{20}$
12	β	1.833	$\frac{1}{12}$	$Pr_{12}O_{22}$	
∞	Dioxide	2.0	0	PrO_2	TbO_2

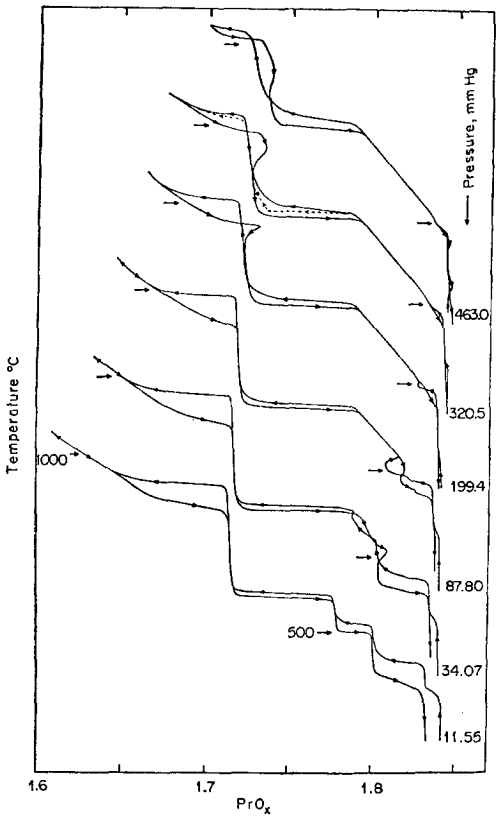

FIG. 1. Representative isobaric runs for the PrO_x (powder)–O_2 system. Pressure indicated in Torr for each run.

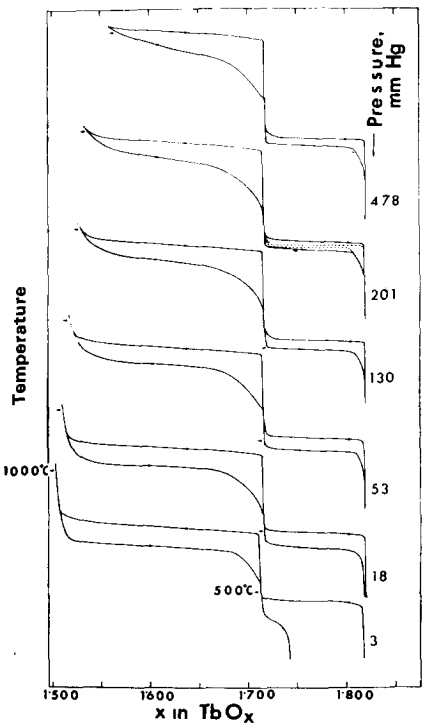

FIG. 2. Representative isobaric runs for the TbO_x (powder)–O_2 system. Pressure indicated in Torr for each run.

before and after the temperature cycling at varied pressures indicated no obvious external changes.

Thermogravimetric analysis was made on a Cahn RG microbalance system with an accuracy of ± 5 μg for a 250 mg sample. The weight, temperature, and pressure were recorded on paper tape every 2 min yielding

TABLE II

ISOBARIC STUDIES OF RARE EARTH OXIDE–OXYGEN REACTIONS IN SINGLE CRYSTALS

Figure number	Mesh size	Crystal diameter (mm)	Pressures (Torr)
		PrO_x	
3	170	0.015 → 0.088	600, 108, 12
4	200	0.088 → 0.074	200, 12
5	200	0.088 → 0.074	83, 47
6	325	0.053 → 0.044	83, 47
7	325, 100, and powder[a]	0.177 → 0.149, 0.053 → 0.044, and powder	47
8	Powder[a]	Powder	47
		TbO_x	
9	100 → 325[b]	0.053 → 0.177	12, 100
10	100 → 325	0.053 → 0.177	47, 400

[a] Ground-up single crystals approximately 0.5 → 1 μm.
[b] 90% of the sample was within this range.

about 1000 points per run. Experimental points were taken by means of the semi-automatic data acquisition system described in (*2*). The data were refined on a CDC 6400 computer and displayed by means of a CALCOMP plotter. Included in this refinement were corrections for thermal flow effects and buoyancy that were determined experimentally using Nd_2O_3 as an inert material at these temperatures and pressures.

Results and Discussion

The PrO_x (Single Crystal)–O_2 System

The isobaric experiments using several sizes of crystals of praseodymium oxide are

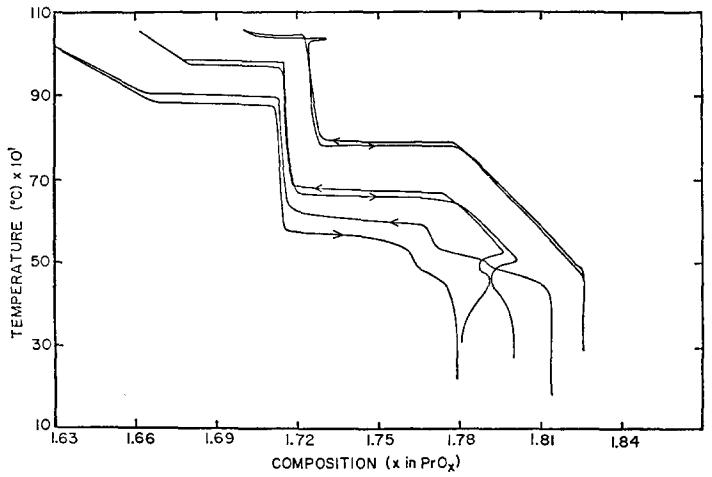

FIG. 3. Isobars of the PrO_x (single crystal)–O_2 system with oxygen pressures left to right: 12, 108, 600 Torr at a mesh size of 170.

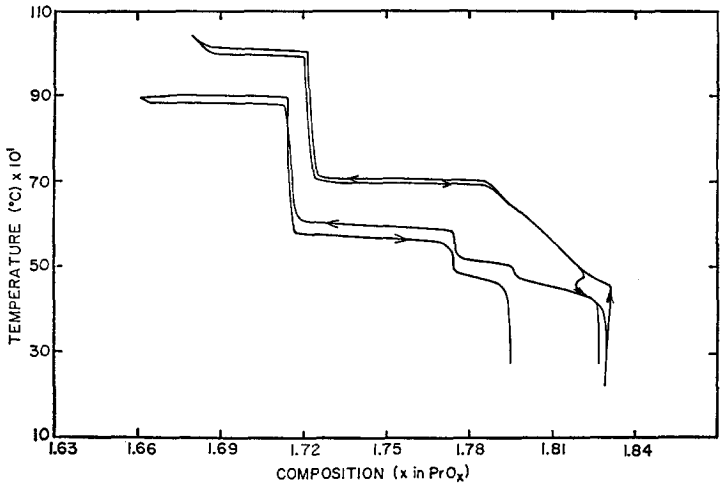

FIG. 4. Isobars of the PrO_x (single crystal)–O_2 system with oxygen pressure left to right: 12 and 200 Torr at a mesh size of 200.

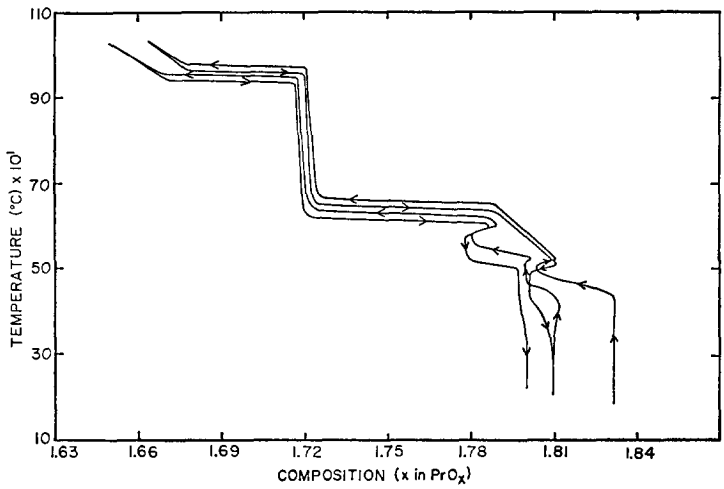

FIG. 5. Isobars of the PrO_x (single crystal)–O_2 system with oxygen pressure left to right: 47 and 83 Torr at a mesh size of 200.

shown in Figs. 3–10. The curves shown are at representative oxygen pressures in each case. The curves are offset toward a more oxidized state with increasing pressure. This pressure dependence is about three times greater than that observed for runs on powder. For all of the runs, the heating and cooling rate is 1°C/min.

The experiments run with 170 mesh (see Table II for diameter range) crystals are shown in Fig. 3. Some of the differences between isobaric runs on powder and single-crystal specimens are immediately obvious. The most striking contrast is that the hysteresis loop in the $\sigma + \imath$ region is much smaller for the single crystals. In addition, the reaction rates were much slower causing the runs to *freeze out* at higher compositions than they did with powders.

Since the oxygen diffusion path is much longer for the single crystals than for the crystallites of the powder [the diffusion

coefficient has been shown to be about the same (5)] equilibrium is not obtained until much higher temperatures are reached. In fact, the cyclic curves at iota do not close at the lowest pressures, a feature never observed for powder samples at these temperatures.

The isobar at 12 Torr shown in Fig. 4 is irreversible over the entire temperature range. Apparently the reaction is slow even at the high temperatures where σ is stable, a feature that disappears at higher pressures.

Upon reduction, the first inflection for the run at 12 Torr is due to a delayed formation of epsilon phase and the second inflection due to zeta phase. In very small crystals (powder) the phase reactions usually are completed sequentially without the complications of simultaneous reactions resulting from diffusion delays. On the other hand, reactions of single crystals may indicate phase reactions greatly shifted in composition and this effect is strongly dependent on

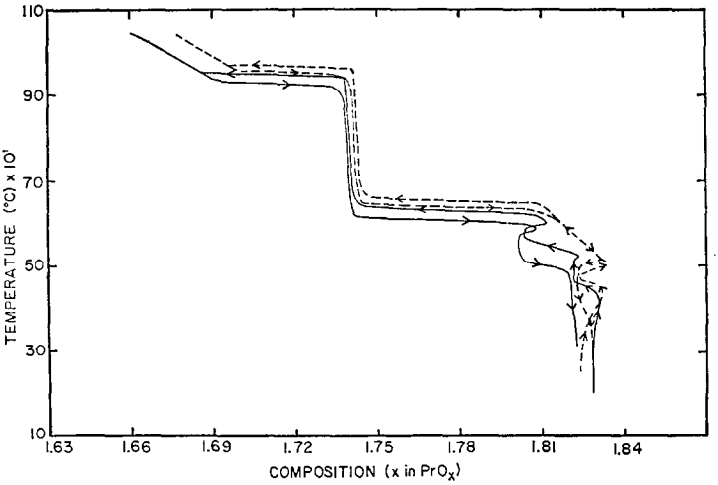

FIG. 6. Isobars of the PrO_x (single crystal)–O_2 system with oxygen pressures left to right: 47 and 83 Torr at a mesh size of 325.

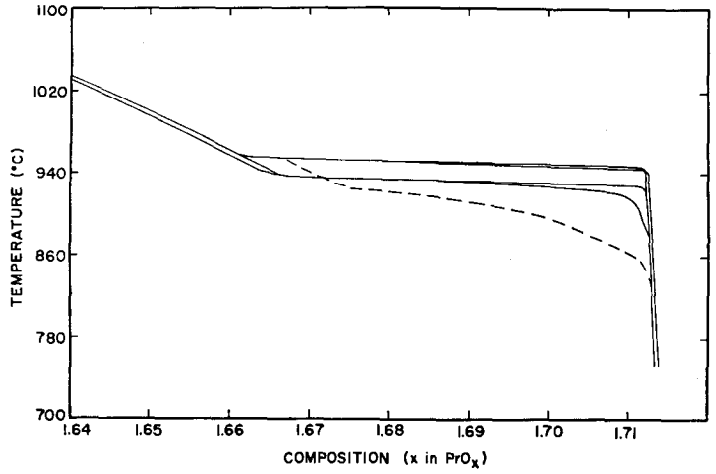

FIG. 7. Isobars of the PrO (single crystal)–O_2 system with mesh sizes of 100, 325, and ground-up single crystal powder (dashed line) at a pressure of 47 Torr.

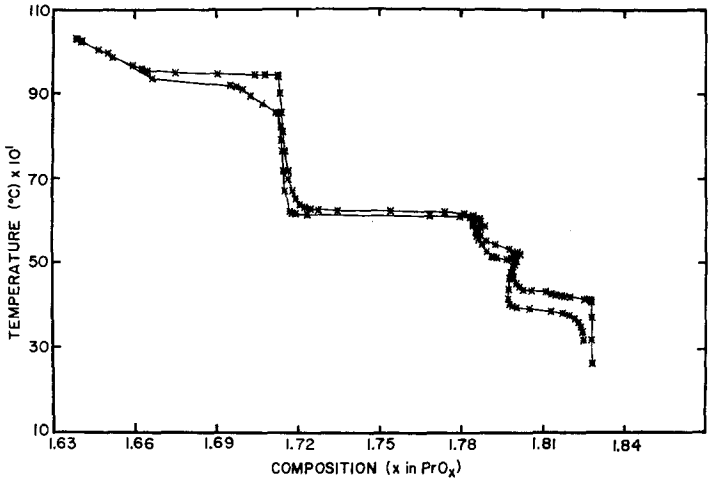

FIG. 8. Isobars of the PrO_x (ground-up crystals)–O_2 system at a pressure of 47 Torr.

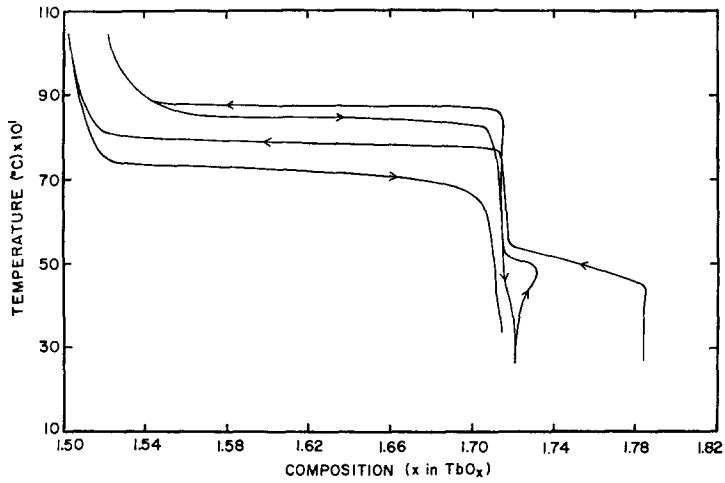

FIG. 9. Isobars of the TbO_x (single crystal)–O_2 system with oxygen pressures left to right: 12 and 100 Torr at mesh sizes of 100 → 325.

crystal size (compare Figs. 3 and 4 for the 12-Torr pressure). During oxidation the curve at zeta phase does not close at all and freezes out soon thereafter; it may at that time consist of both zeta and epsilon phases. Following a low-temperature oxidation the cycle at 108 Torr indicates a reduction to epsilon phase. In the oxidation cycle in this region the α phase formed is more oxidized at all temperatures. This crossover may result from the formation of an α phase of different properties when formed from iota rather than from either ε or β (*6*).

The apparent overshoot out of $\sigma + \iota$ into α shown by the horizontal spoke at the highest pressure run (600 Torr), is much less pronounced and much sharper than in powder runs. It results from the oxidation of a metastable σ to α, which subsequently decomposes to ι (*7*).

Heating cycles made at 200 Torr and 12 Torr for 200-mesh crystals are shown in

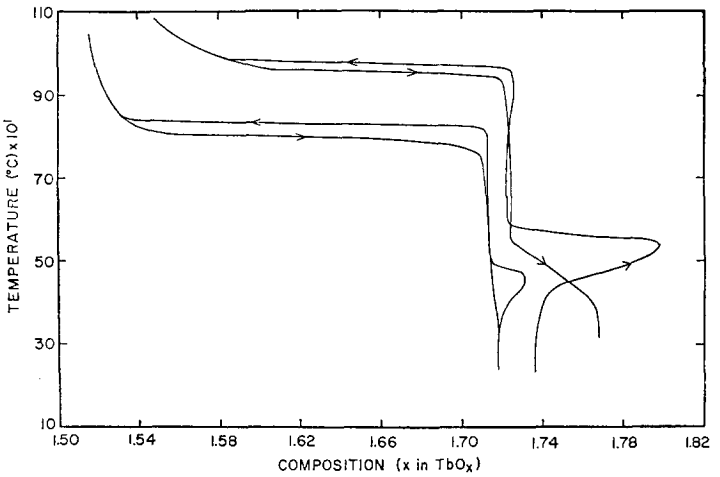

FIG. 10. Isobars of the TbO_x (single crystal)–O_2 system with pressures left to right: 47 and 400 Torr at mesh sizes of 100 → 325.

Fig. 4. In the 200-Torr run, there is no overshoot into the α region upon cooling from the σ phase, in contrast to powder runs (Fig. 1). In the 12-Torr isobar, closure of the curves at ζ is not quite complete and the system freezes out at a composition near ε. The apparent ζ composition occurs again at a high value, probably due in reduction to some formation of ι and in oxidation to slow reaction rate.

Further runs on 200-mesh crystals made at 83 and 47 Torr are shown in Fig. 5. The 83-Torr run is started at the composition of $PrO_{1.833}$ and it ends at a composition near $PrO_{1.81}$. The next run at 47 Torr begins at $PrO_{1.81}$ and ends at an even lower composition—emphasizing the marked slowness of the reaction compared to the powders which would all have reoxidized to $PrO_{1.833}$. In both runs, there is a wide and distinct epsilon phase near the composition of $PrO_{1.800}$, the apparent stability range being much broader than for the powder. This difference in behavior results from marked reduction in pseudophase formation at any part of the range. The curves fail to close at the α and ι phases and the hysteresis loop between σ and ι remains very small.

Runs carried out at similar pressures but with smaller crystals (325-mesh) are shown in Fig. 6. The difference between a 200-mesh run and a 325-mesh run appears to be slight, with the important exception that the hysteresis loops in Fig. 6 seem to be slightly larger and there is a definite appearance of pseudophase formation.

A sample of 200-mesh crystals was ground under liquid nitrogen to determine whether the large isobaric hysteresis loop would reappear using a specimen of reduced crystallite size. Examination under the microscope indicated that the average size of the shattered crystals was approximately 0.5–1 μm, only five to ten times the diameter of the particles of powder.

The dashed line in Fig. 7 shows the return of the large hysteresis loop and the pseudophase. This figure shows clearly the progressive development of the loop and pseudophase on reduction of crystallite size.

The transformation temperatures for ground-up single crystals were lower than for the larger crystals. The dashed line was overlaid at the same transformation temperature for size comparisons only.

The specimen of ground-up crystals was cycled at 47 Torr, as illustrated in Fig. 8. These curves are intermediate in appearance between those of larger crystals and powdered samples with the clear appearance of larger hysteresis loops, more pseudophase behavior not only in the $\sigma\iota$ region but also in the hyperstoichiometric region of ζ and ε. Note also

that reoxidation of the sample nearly to the composition of β is achieved.

The TbO_x (Single Crystal)–O_2 System

Due to the limited quantity of terbium oxide single crystals available, a series of isobars was run with a mixture of crystal sizes between 100 and 325-mesh. This also enabled a comparison between single-crystal and powder behavior in the TbO_x–O_2 system. Isobars carried out at 12 and 100 Torr are shown in Fig. 9. The lower pressure run is started at a composition much below δ and in oxidation it never gets beyond the ι phase. In the run at 100 Torr there is a slight initial oxidation on heating. The reduced reaction rates of the system are again in contrast to the powder TbO_x–O_2 system and as found in PrO_x single crystals the hysteresis loop between φ and ι is much reduced in size.

In Fig. 10 runs at 47 and 400 Torr are shown for the same specimen. The starting composition in both reductions is more oxidized than ι and oxidation beyond ι occurs only at the highest pressure on cooling. Besides the marked reduction in reaction rates caused by long diffusion paths and marked at lower temperatures the temperature at which reduction of ι occurs is lower for the single crystals and, as observed with the PrO_x system, the hysteresis loop is greatly reduced in size. The occurrence of some pseudophase could be credited to some crystals of small size and to a reduced reaction rate for TbO_x.

Concluding Remarks

Hysteresis, which depends on the rate of traversal in phase transitions of rare earth oxides, could result from a slow rearrangement of metal atoms at the phase boundary, slow diffusion of oxygen through the solid to or from the reaction boundary, or nucleation of the new phase. Whatever the cause the effect is enhanced at lower temperatures and oxygen pressures.

Intrinsic hysteresis could be due to an impurity in the sample stabilizing one of the phases, a rapid nucleation process that changes the transformation temperature, or an interfacial free energy being different in the oxidation path and reduction path.

For the lower temperature phase transitions in both the TbO_x–O_2 system and the PrO_x–O_2 system (below iota composition) the reaction paths are determined to some degree by the rate of temperature change. It would appear probable that the increased diffusion path length for oxygen in the larger crystals and the variation of the oxygen chemical potential gradient accounts for these kinetic effects including the freeze-out of the phases at lower temperature.

If the upper temperature loop [$\iota + \varphi(\sigma)$ in TbO_x, $\iota + \sigma$ in PrO_x] was also rate-dependent, one would expect enhanced hysteresis for larger crystals, but just the opposite occurs—the larger the crystals the smaller the loop. Along with the studies on TbO_x powder there is then substantial evidence that this high temperature loop is indeed independent of rate of temperature change except for TbO_x at the lowest pressures.

The clear relationship between the size of the crystals and the size of the hysteresis loop suggests the influence of an exterior surface term related to nucleation processes. A set of experiments on the effect of particle size by Natarajan *et al.* (*8*) revealed that, as observed here, the larger the crystal size the smaller the hysteresis loop (a linear relationship) and the lower the transition temperature. However, in this case the size of the loops was found to be dependent of the rate of temperature change. These trends were interpreted by Natarajan *et al.* (*8*) in terms of Turnbull's theory of heterogeneous nucleation (*9*), in which the rate of nucleation is proportional to the amount of nucleation surface. This is not inconsistent with the results of the lower temperature phases of the TbO_x–O_2 and PrO_x–O_2 systems, in which there is a slower reaction of the new phase for the larger crystals (less surface). However, note that the same results can be explained in terms of the increased diffusion path and/or a change in the chemical potential gradient of the diffusing species.

On the other hand hysteresis loops occurring at higher temperatures (such as between ι and φ) appear to be independent of the variation

of the rate of temperature change. This eliminates rate-dependent nucleation or propagation as an explanation for this type of hysteresis. Furthermore, as was pointed out by Kröger (*10*), if nucleation retardation were responsible, once enough nuclei were formed there would be a return to the true transition temperature—contrary to experience. The theory must include consideration of the metastable coexistence of two phases.

If nucleation is preferentially initiated on the surface of the crystal, there should be fewer nucleation sites in the larger crystals. Since it is believed that at sufficiently high diffusion rates oxygen is in equilibrium with the entire solid, preferential nucleation is dependent on some type of exterior surface effect. Since the new phase being nucleated as a different lattice parameter than the matrix, there will be less strain at the surface; hence, nucleation would be more likely to occur there. Therefore, since there is less surface per unit mass in the large crystals, there will be fewer nuclei per unit mass. As a result fewer and larger domains will grow from the surface inward in the case of larger crystals at the same composition. A larger domain results in a smaller interfacial effect (less strain) between the two phases, and therefore, in a smaller hysteresis loop for the larger crystals.

This would also explain the decreased extent of pseudophase formation believed to result from strained isolated *islands* of reactant in a matrix of product in the larger crystals. There would be fewer of these isolated islands of φ phase, for example, in the pseudophase region for the larger crystals because of the reduced number of nucleation sites. This effect would be expected for hyperstoichiometric regions as well, as is indeed the case.

Acknowledgment

It is our pleasure to acknowledge the full support of the United States Atomic Energy Commission in the performance of these experiments.

References

1. M. Z. Lowenstein, L. Kihlborg, K. H. Lau, J. M. Haschke, and L. Eyring, *Proc. NBS Spec. Pub.* **364**, 343 (1972).
2. A. T. Lowe and L. Eyring, *J. Solid State Chem.* (1974).
3. J. Kordis and L. Eyring, *J. Phys. Chem.* **72**, 2044 (1968).
4. J. Haschke and L. Eyring, *J. Inorg. Chem.* **10**, 2267 (1971).
5. K. H. Lau, D. Fox, S. H. Lin, and L. Eyring, to appear.
6. M. S. Jenkins, R. P. Turcotte, and L. Eyring, "The Chemistry of Extended Defects in Non-Metallic Solids" (L. Eyring and M. O'Keeffe, Eds.), p. 36, North-Holland, Amsterdam (1970).
7. B. G. Hyde, D. J. M. Bevan, and L. Eyring, *Philos. Trans. Roy. Soc. London Ser. A.* **259**, No. 1106, 583 (1966).
8. M. Natarajan, A. R. Das, and C. N. R. Rao, *Trans. Faraday Soc.* **58**, 1579 (1962).
9. D. Turnbull, *J. Chem. Phys.* **17**, 71 (1949); **18**, 198, 768, 769 (1950).
10. F. A. Kröger, "The Chemistry of Imperfect Crystals," p. 993, North-Holland, Amsterdam (1964).